#### **ARTICLE IN PRESS**

Environmental Research xxx (xxxx) xxx

ELSEVIER

Contents lists available at ScienceDirect

#### **Environmental Research**

journal homepage: www.elsevier.com/locate/envres



## Investigating the microstructure of high-calcium fly ash-based alkali-activated material for aqueous Zn sorption

Sukanta K. Mondal <sup>a,b</sup>, Adam Welz <sup>a,b</sup>, Ali Rownaghi <sup>b</sup>, Bu Wang <sup>c</sup>, Hongyan Ma <sup>d</sup>, Fateme Rezaei <sup>b</sup>, Aditya Kumar <sup>e</sup>, Monday U. Okoronkwo <sup>a,b,\*</sup>

- <sup>a</sup> Sustainable Materials Laboratory (SusMatLab), Missouri University of Science and Technology, Rolla, MO, 65409, United States
- b Department of Chemical and Biochemical Engineering, Missouri University of Science and Technology, Rolla, MO, 65409, United States
- <sup>c</sup> Department of Civil & Environment Engineering, University of Wisconsin—Madison, Madison, WI, 53706, United States
- d Department of Civil, Architectural & Environmental Engineering, Missouri University of Science and Technology, Rolla, MO, 65409, United States
- e Department of Materials Science and Engineering, Missouri University of Science and Technology, Rolla, MO, 65409, United States

#### ARTICLE INFO

# Keywords: Heavy metals Zinc Adsorption Alkali-activated materials Thermodynamic modeling

#### ABSTRACT

The performance of adsorbents prepared by alkali activation of high calcium fly ash was investigated for removing aqueous Zn. Two formulations involving the use of NaOH and  $Na_2SiO_3$  activating solutions were used to prepare the adsorbents that feature different microstructural characteristics. The Zn sorption data indicates a sorption process that is controlled by both chemisorption and intra-particle diffusion. The  $Na_2SiO_3$ -activated material displayed higher sorption rates compared to the NaOH-activated material. The sorption kinetics show strong dependence on the microstructures of the adsorbents, wherein the  $Na_2SiO_3$ -activated material featuring higher contents of amorphous phases (96  $%_{mass}$ ) in the hydrated phase assemblage, with attendant improved porosity and surface area, performed better than the NaOH-activated material (86  $%_{mass}$  amorphous phases) which showed higher degree of crystallinity and coarse morphology. The  $Na_2SiO_3$ -activated material exhibited 100% Zn removal efficiency within the first 5 min in all studied initial adsorbate concentrations(corresponding to sorption capacity of up to 200 mg/g), while the NaOH-activated analogue tends to lag, reaching 99.99% Zn removal efficiency after about 240 min in most cases. The two formulations were also examined with thermodynamic modeling and the results agree with experimental data in indicating that the use of alkali-silicate activating solution is most suitable for converting high calcium fly ash into efficient adsorbent for removing aqueous heavy metals.

#### 1. Introduction

The development of new adsorbents derived from industrial (Gupta et al., 2003; Hegazi, 2013; De Gisi et al., 2016) and agricultural (Hegazi, 2013; Malik et al., 2017) wastes, natural materials (Erdem et al., 2004; Abu-Eishah, 2008; Elouear et al., 2008), and biopolymers (Kumar and Jiang, 2016; Zhang et al., 2016) for the sorption of aqueous heavy metal has gained increased research attention in recent decades (Babel and Kurniawan, 2003; Ahmed and Ahmaruzzaman, 2016), owing to the attractive properties such as eco- and cost-efficiency, high sorption capacities, simplicity and a broad pH range suitability exhibited by these new materials (Barakat, 2011). However, despite the attractiveness and the potentials to improve the properties, their general acceptability in the wastewater treatment industry is limited due to the existence of

unanswered questions about the materials' behavior. Thus, conventional and more costly adsorbents (e.g., carbon-, and metal-based adsorbents) have remained as leading adsorbents used in practice (Barakat, 2011; Bolisetty et al., 2019; Roy, 1994).

Alkali-activated materials (or geopolymers) are promising low-cost adsorbents prepared from precursor aluminosilicates, e.g., fly ash, an abundant waste product of coal combustion (Adriano et al., 1980; Ahmaruzzaman, 2010; Mondal et al., 2020). The geopolymer material is composed mainly of a three-dimensional inorganic polymeric gel (Davidovits, 1991), which often transforms to crystalline zeolites at appropriate reaction conditions (e.g., high temperature and pressure) (Provis et al., 2005). Owing to the material's unique physicochemical properties, it exhibits significantly high sorption capacity for a variety of heavy metals (Al-Harahsheh et al., 2015; Mondal et al., 2020; Siyal

https://doi.org/10.1016/j.envres.2020.110484

Received 23 July 2020; Received in revised form 29 September 2020; Accepted 11 November 2020 Available online 17 November 2020 0013-9351/© 2020 Elsevier Inc. All rights reserved.

<sup>\*</sup> Corresponding author. Department of Chemical and Biochemical Engineering, Missouri University of Science and Technology, Rolla, MO, 65409, United States. E-mail address: okoronkwom@mst.edu (M.U. Okoronkwo).

et al., 2018), including Zn (Kara et al., 2017): it can remove most heavy metal ions by multiple mechanisms including sorption, immobilization by structural incorporation and physical encapsulation (El-Eswed, 2018; Okoronkwo et al., 2018; Pereira et al., 2009; Provis, 2009).

The growing global anthropogenic activities have led to an upsurge in the amount of heavy metal discharged into the environment. Zinc is one of the heavy metals present in effluents from various industries, including metallurgical and battery manufacturing industries (Fu and Wang, 2011; Hojati and Landi, 2015). Although Zn is one of the essential minerals needed for proper function of the human body, an excessive amount of Zn can be toxic to aquatic organisms and humans (Clancey and Murphy, 2012; Graham et al., 1991; 1987; Hart and BT, 1974; Nordberg et al., 2014; Plum et al., 2010), hence the World Health Organization imposed legal limit of 5 mg Zn/L.

Low calcium fly ashes corresponding to the ASTM C618 Type F (with CaO  $<18~\mbox{$M_{\rm mass}$}$ ) (ASTM C618, 2019), are the most widely studied class of fly ash for the synthesis of geopolymers for both sorbent and structural applications (Duxson et al., 2007; Provis and Deventer, 2014; Shi, 2019; Tan et al., 2020), arguably because of its higher pozzolanic activity and geopolymerization rate. Conversely, the alkali-activated high-Ca fly ash, which forms predominantly a geopolymer-like calcium-alkali-aluminum-silicate-hydrate gel [i.e., C-(N)-A-S-H gel when activated with sodium-based alkaline solution](Bernal et al., 2014; Myers et al., 2014), and minor crystalline cement hydrate phases and zeolite, is rarely used for the synthesis of geopolymer-based adsorbents. Thus, there are limited studies in literature focusing on alkali-activated high calcium fly ash as an adsorbent for metal sorption. Therefore, we

present a study of adsorbent derived from alkali-activation of high-Ca fly ash, with a focus on understanding the best formulation protocol to successfully convert the precursor into highly efficient sorbent for removing aqueous Zn. Emphasis is placed to investigate the evolution of sorption kinetics and efficiency as a function of microstructural development.

#### 2. Experimental program

#### 2.1. Material preparation

The major oxide composition of the high Ca precursor fly ash, i.e., Type C fly ash (ASTM C618, 2019) used for the current study is as follows: 33.61% CaO, 33.81% SiO<sub>2</sub>, 17.42% Al<sub>2</sub>O<sub>3</sub>, 6.35% Fe<sub>2</sub>O<sub>3</sub>, 5.46% MgO, 1.82% SO<sub>3</sub>, 0.98% Na<sub>2</sub>O, 0.56% K<sub>2</sub>O (mass basis). Two different adsorbents were formulated by reacting the fly ash with both 10 M NaOH and 1 M Na<sub>2</sub>SiO<sub>3</sub> solutions (Gunasekara et al., 2015; Van Jaarsveld et al., 2002) at a solution-to-solid mass ratio of 0.7, with stirring at 850 rpm at ambient condition for 20 min. After the 20 min stirring time, the resulting pastes were placed in an oven where they were cured at 90 °C for 24 h, and then aged for 7 days at room temperature, in sealed plastic cubes. It is noted that while the 10 M NaOH solution chosen for the activation has been reported as relatively more effective in activating the dissolution of fly ash and consequent precipitation of hydration products (Rattanasak and Chindaprasirt, 2009), the Na<sub>2</sub>SiO<sub>3</sub> solution concentration used singly in the present study is uncommon in literature but it produced a beneficial high amorphous adsorbent as

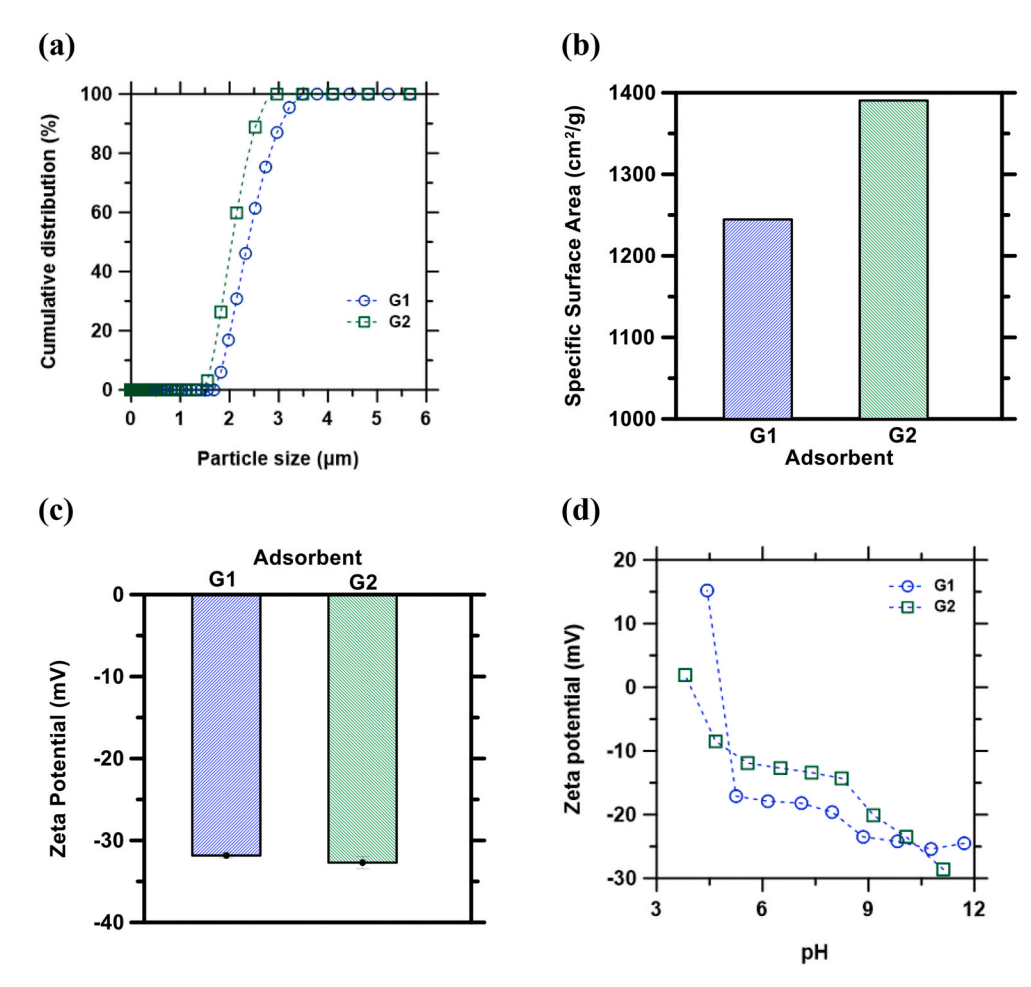


Fig. 1. (a) Particle size distribution of pulverized adsorbent samples used for adsorption studies, (b) Specific surface area of the adsorbent particles, (c) Zeta-potential of the adsorbent particles dispersed in deionized water (pH  $\sim$  13), (d) Zeta-potential of the adsorbent particles as a function of pH. Dotted lines are "visual guides". G1 = Adsorbent synthesized with NaOH; G2 = Adsorbent synthesized with NaOH; G2 = Adsorbent synthesized with NaOH; G3 = Adsorbent synth

discussed in a later section. After seven days of aging, the prepared adsorbents were grounded with the aid of mortar and pestle prior to characterization by Fourier-Transform Infrared Spectroscopy (FTIR), X-ray Powder Diffraction (XRD), Scanning Electron Microscopy (SEM), and Dynamic Light Scattering (DLS) methods.

Fig. 1a displays the particle size distribution (PSD) and Fig. 1c the zeta potential ( $\zeta$ ) of the synthesized adsorbents, showing similar PSD and zeta potential ( $\zeta$  comparable to previous studies (Gunasekara et al., 2015)) for the synthesized G1 and G2 adsorbents (where G1 = Adsorbent synthesized with NaOH; G2 = Adsorbent synthesized with Na<sub>2</sub>SiO<sub>3</sub> solution). Fig. 1b shows the specific surface areas of G1 and G2 (i.e., 1244.63 cm<sup>2</sup>/g and 1390.43 cm<sup>2</sup>/g, respectively) calculated from measured particle distribution and density of the adsorbents, while Fig. 1d displays the evolution of zeta potential of both synthesized adsorbents as a function of pH, showing that the surface charge of both adsorbents are sufficiently negative at chosen sorption pH of 6 (described in section 2.3), thus enhancing the dispersion and electrostatic interaction between adsorbent surfaces and the positively charged adsorbate ion (i.e., Zn<sup>2+</sup>) to improve Zn removal (He and Xie, 2018; Savaji et al., 2014).

#### 2.2. Analytical methods

The particle size distribution (PSD) was measured with Anton Paar Litesizer™ 500 dynamic light scattering (DLS) instrument. Isopropanol was used as the dispersion media, and the solute-to-solvent ratio was maintained at 0.0006 g/mL. Also, the zeta potential of the adsorbent dispersed in deionized water was measured using the Litesizer™ 500, and as a function of pH with the aid of Metrohm 800-Dosino (a dosing units for automated pH adjustment). The specific surface areas (SSA) of the adsorbent samples were determined using the PSD and the density of the adsorbents measured using Ultrapyc 1200e Pycnometer. It is noted that although the method for SSA estimation uses the assumption of a spherical particle aggregate similar to the inbuilt model in the dynamic light scattering protocol, the uncertainty in relative values of SSA for the two samples treated alike is negligible.

An Oxford X-Supreme 8000 X-ray fluorescence (XRF) spectrometer was used to analyze the oxide composition of the fly ash. The mineral phase assemblage of the fly ash and the synthesized geopolymers were examined by powder XRD (PANalytical X'Pert Pro Multi-Purpose Diffractometer) in a 20 arrangement utilizing CuK $\alpha$  radiation (wavelength  $\lambda=1.540$  Å). The samples were scanned from  $5^{\circ}$ -to- $90^{\circ}$  20 in a continuous manner at a step size of  $0.026^{\circ}$  20. The morphology of the prepared adsorbents were imagined using a scanning electron microscope (SEM, Hitachi S4700), while a voltage of 10 kV was applied. To prevent charging, the samples collected on carbon-taped brass studs were gold-coated prior to SEM analyses. The infrared spectra of selected samples were measured using Attenuated Total Reflection (ATR) approach with a Nicolet iS50 FT-IR spectrometer equipped with a diamond cell. FTIR spectra was measured from wavenumber of 400-to- $4000~{\rm cm}^{-1}$  with the resolution set at 4 cm $^{-1}$ .

The aqueous elemental Zn were measured with PerkinElmer AVIO 200 Inductively Coupled Plasma - Optical Emission Spectrometer (ICPOES) equipped with a concentric glass nebulizer. The solution samples were introduced at 2.0 mL min $^{-1}$  using a PerkinElmer S10 Autosampler. The spectra line of the elemental Zn 213.856 nm was measured and the mean of triplicate measurements of the aqueous elemental Zn was obtained. The detection limit for the ICP-OES is 0.1 ppm-to-100 ppm. Selected samples with Zn concentrations  $\approx$  zero (i.e., indicating 100% Zn uptake) were verified with Graphite Furnace Atomic Absorption Spectrophotometer (GFAA, model Analyst 600, PerkinElmer), wherein the detection limit of the GFAA is in the order of part per billion (ppb) for most metal and semi-metal elements.

#### 2.3. Sorption tests

Batch sorption experiments were performed using both 100-ppm and 200-ppm Zn solutions prepared from reagent grade Zn(NO<sub>3</sub>)<sub>2</sub> and deionized water (18.2 MΩ-cm). An adsorbent dosage of 2 g/L was studied for the 100-ppm system, while adsorbent dosages of 1 g/L and 2 g/L were studied for the 200-ppm solution. The initial Zn concentrations and adsorbent dosages were selected based on the conditions commonly reported as optimum for Zn removal using geopolymer, a similar material made from alkali-activation of low-Ca aluminosilicates (Al-Harahsheh et al., 2015; Al-Zboon et al., 2016; Kara et al., 2017). For each setup, Zn sorption was examined as a function of contact time by analysis of filtered aliquot samples taken from the batch experiments at regular intervals from 5 min-to-240 min. A fixed temperature of 40 °C and pH 6 reported as optimum in related stusies (Al-Harahsheh et al., 2015; He et al., 2016) was maintained for the sorption experiment, while the system was stirred at 300 rpm. Also, the pH 6 is selected for the present study because, as noted in section 2.1 (Fig. 1d), the adsorbents feature a reasonable negative surface charge ( $\zeta > -10$  mV) at pH 6 which improves the particles dispersion and electrostatic interaction with the positively charged Zn<sup>2+</sup> to aid the sorption process. The aliquot samples collected at regular time intervals were filtered through a 0.2-µm PTFE syringe filter, diluted with 3% nitric acid prior to elemental Zn analysis by ICP-OES. The Zn removal efficiency (%) of the prepared adsorbents were calculated with equation (1) (Al-Zboon et al., 2011; Ge et al.,

Zinc removal efficiency (%) = 
$$\frac{C_i - C_{eq}}{C_i} \times 100$$
 (1)

where  $C_i$  is the initial concentration of Zn (ppm),  $C_{eq}$  is the equilibrium concentration of Zn (ppm) in sorption solution. The time-dependent Zn uptake (mg/g) by the adsorbents were calculated with equation (2) (Uddin et al., 2017; Xu et al., 2008):

$$q_{t} = \frac{(C_{i} - C_{eq}) \times V_{s}}{m}$$
 (2)

where  $q_t$  is the time-dependent Zn uptake per gram of adsorbent (mg/g),  $V_s =$  the volume of the sorption solution (L), and m = the mass of adsorbent (g).

#### 2.4. Simulation method

The mineral phase assemblage in the adsorbents was also examined by thermodynamic modeling as a function of fly ash degree of reaction. The simulations were performed with the Gibbs Energy Minimization Software (GEMS, version 3) (Kulik et al., 2013), which is a geochemical modeling code developed at Paul Scherrer Institute. The software uses the principles of Gibbs energy minimization in computing the equilibrium reaction product (i.e., phase assemblages) and the ionic speciation. The code uses the reactants composition and the thermodynamic properties of the chemical species to calculate the equilibrium chemical reaction product balances. The thermodynamic properties of relevant phases for the present study were curated from the default database built into the GEMS platform(Hummel et al., 2002; Johnson et al., 1992; Thoenen et al., 2013), the cement database (CEMDATA18) (Lothenbach et al., 2019), and the Thermoddem thermodynamic database for zeolites (Blanc et al, 2012, 2015). The effects of solution non-ideality resulting from the presence of dissolved salts was accounted for with the Truesdell-Jones form of the extended Debye-Hückel model (Equation (3)) (Helgeson et al., 1970).

$$\log \gamma_j = \frac{-Az_j^2 \sqrt{I}}{1 + B\alpha_i \sqrt{I}} + bI + \log_{10} \frac{x_{jw}}{X_w}$$
(3)

where,  $\gamma_i$  = the activity coefficient of jth ion; I = the ionic strength of the

solution (mol·kg<sup>-1</sup>);  $x_{jw}$  = the molar quantity of water, and  $X_w$  = the total molar amount of the aqueous phase.  $z_j$  = the charge of jth ion;  $\alpha_j$  effective hydrated diameter of jth ion (set at 3.31 Å for NaOH-dominated solution); A and B are temperature and pressure dependent Debye-Hückel electrostatic parameters (units of kg<sup>1/2</sup> mol<sup>-1/2</sup> and kg<sup>1/2</sup> mol<sup>-1/2</sup> m<sup>-1</sup>, respectively (Hummel et al., 2002); b is a semi-empirical parameter that describes short-range interactions between charged aqueous species, set at 0.098 kg/mol for a NaOH-dominated solution (Helgeson et al., 1981). It is noted that beyond ionic strengths of 2.0 mol/L for the starting solution, absolute values of calculated material balances may feature minor uncertainties proportional to the ionic strength, but the trends of the calculated quantities are correct (Kulik et al., 2013).

#### 3. Results and discussion

#### 3.1. Kinetics, efficiency, and mechanism of Zn sorption

The uptake of Zn by the prepared adsorbents as a function of contact time (i.e., the adsorbent's resident time in the adsorbate solution), for the three different batch sorption experimental set ups are shown in Fig. 2. The Zn uptake by the materials, as seen, was very rapid, especially for G2 (Adsorbent prepared with Na2SiO3), where 100% of the Zn had been removed within the first 5 min of the material's contact with the Zn solution, in all three systems studied. Although G1 (Adsorbent prepared with NaOH) showed a slower rate of Zn uptake compared to G2, it also displayed a remarkably high removal efficiency compared to previous studies (Al-Zboon et al., 2016; Erto et al., 2015; Hojati and Landi, 2015; Kara et al., 2017): it featured an average of 99.41% removal efficiency at contact time of 5 min which increased with time, catching up with the performance of G2 at about 240 min (Fig. 3a). Table 1 compares the result of the Zn sorption in this study with those of previous studies of related materials. The results in this study indicate that, while the equilibrium Zn uptake per gram of adsorbent show similar linear proportionality scales with the initial Zn concentrations for both G1 and G2 (Fig. 3b), the kinetics of the sorption process is more complex and evidently material dependent - implications of which is discussed in section 3.2.

Hence, the selection of appropriate formulation protocol is critical for designing efficient high-Ca fly ash based adsorbents for specific applications. For instance the  $\rm Na_2SiO_3$ -activation method used to prepare G2 would be preferable for making adsorbent water filters for which a rapid sorption is needed and contact time is expected in the range of seconds-to-few minutes, whereas for certain industrial effluent

treatment applications where contact times in the range of minutes-to-hours are allowable, either formulation methods employed for G1 and G2 preparation would suffice to convert the high-Ca fly ash to "purposed-efficient" adsorbent.

To investigate the mechanism of the Zn sorption process, the results were analyzed using various kinetic models. As shown in Fig. 4, the data from all the experiments show excellent fit to the pseudo-second-order kinetic model given in equation (4), with coefficients of determination  $R^2 \approx 1.00$ , in agreement with similar studies (Al-Harahsheh et al., 2015; Gupta and Bhattacharyya, 2011; Uddin et al., 2017), suggesting a chemisorption-controlled sorption process (Ho, 2006; Ho and McKay, 1999; Juang et al., 2002). The estimated pseudo-second-order rate constant,  $k_2$ , tends to infinity for the Na<sub>2</sub>SiO<sub>3</sub>-activated material (G2) compared to the NaOH-activated material (G1) which yielded a lower rate constant  $k_2$  in the range 0.024–5.89 (Fig. 4).

Second order: 
$$\frac{t}{q_t} = \frac{1}{k_2 q_e^2} + \frac{1}{q_e} t$$
 (4)

where  $q_t$  is the time-dependent Zn uptake per gram of adsorbent (mg/g), and  $q_e$  is the uptake at equilibrium. The sorption data was also examined with the simplified Elovich's equation which has been extensively applied to describe chemisorption processes (Aharoni and Tompkins, 1970; Juang and Chen, 1997; Wu et al., 2009a) (equation (5)), and the Intra-particle diffusion (IPD) model shown in equation (6) (Simonin and Bouté, 2016; Wu et al., 2009b).

Elovich's equation : 
$$q_t = \frac{1}{b}\ln(ab) + \frac{1}{b}\ln(t)$$
 (5)

where a = the initial adsorption rate (mg/g.min), and the constant b (g/mg) is often referred to as the desorption constant and have been thought to be related to the degree of surface covered and the activation energy of chemisorption process (Örnek et al., 2007; Riahi et al., 2017).

IPD model: 
$$q_t = k_{id} \cdot t^{1/2} + \theta$$
 (6)

where  $k_{id}$  is the intra-particle diffusion rate constant (mg/g·min<sup>1/2</sup>),  $\theta$  (mg/g) is a constant correlated to the boundary layer thickness (Fierro et al., 2008; Kannan and Sundaram, 2001).

Data from the first-two batches of the sorption experiments, (i.e.,  $100 \, \text{ppm} \, \text{Zn}$  initial concentration –  $2 \, \text{g/L}$  adsorbent dosage; and  $200 \, \text{ppm} \, \text{Zn}$  initial concentration –  $2 \, \text{g/L}$  adsorbent dosage) did not fit well to the Elovich and IPD models: this is thought to be due to (i) insufficient data points, as uptake of Zn was very rapid, more data points are needed from the intervals of 0-to-5min, to clearly describe these batches (e.g., G1 in

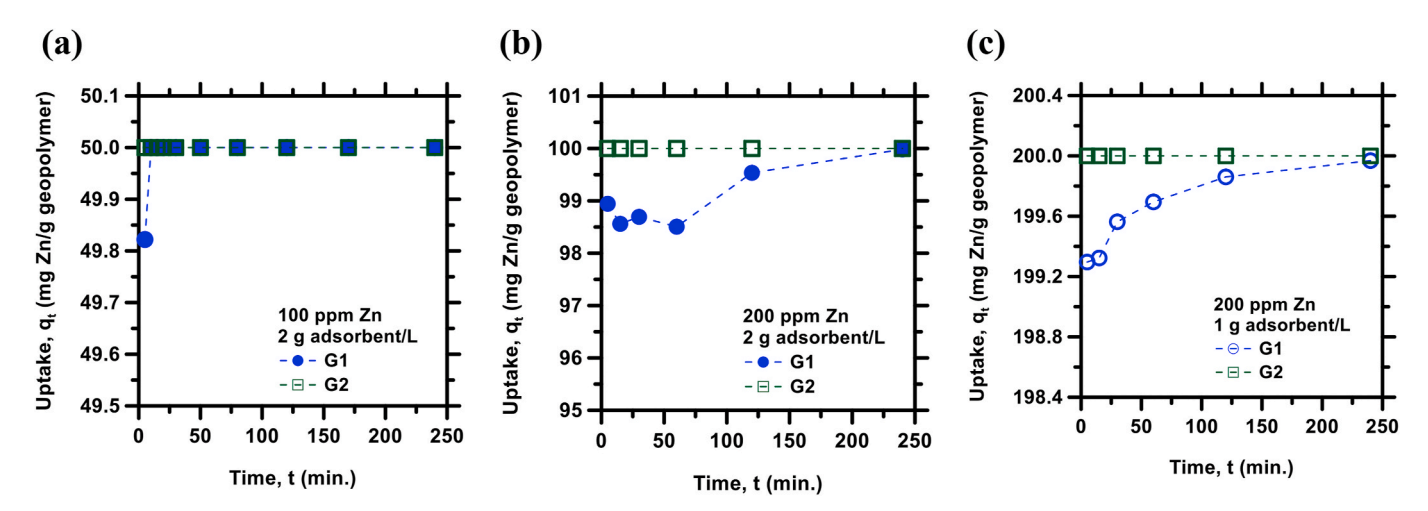
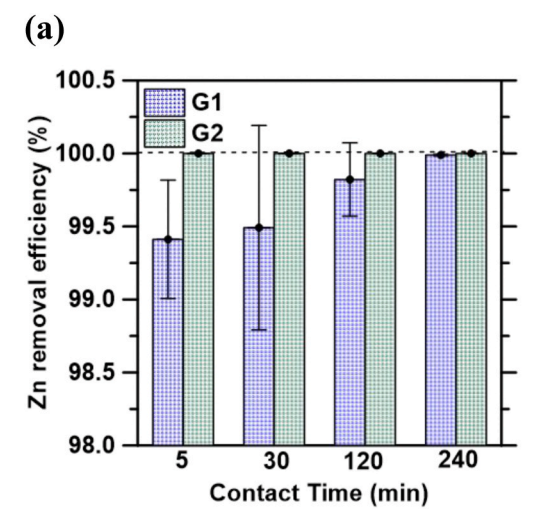


Fig. 2. Zn removal as a function of time for the different sorption set ups with initial Zn concentrations and adsorbent dosages of: (a) 100 ppm and 2 g/L; (b) 200 ppm and 2 g/L; and (c) 200 ppm and 1 g/L, respectively. G1 = Adsorbent synthesized with NaOH; G2 = Adsorbent synthesized with Na2SiO<sub>3</sub>. The dotted lines are "visual guides".



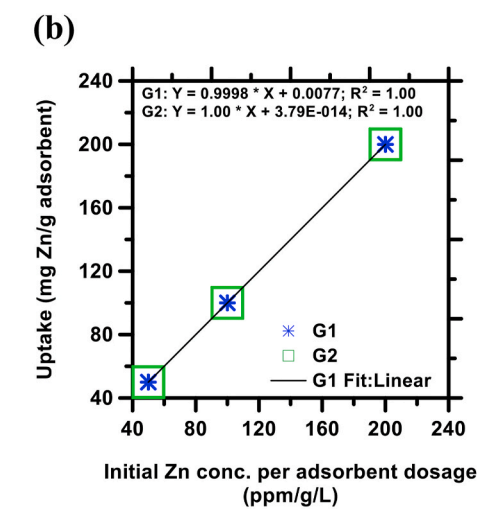


Fig. 3. (a)Time-dependency of the Zn sorption efficiency, (b) Uptake (sorption capacity) as a function of initial Zn concentration per adsorbent dosage: Error bars are standard deviation of data from the three sorption set up (i.e., with initial Zn concentrations and adsorbent dosages of 100 ppm and 2 g/L; 200 ppm and 2 g/L; and 200 ppm and 1 g/L, respectively.

Table 1

Zn sorption results reported for related alkali-activated (geopolymer) materials

Alkali- activated adsorbent material (or Geopolymer)	Adsorption capacity, $q_m$ (mg Zn/g adsorbent)	Zn removal efficiency (%)	Sorption (optimum) conditions	References
Natural volcanic tuff based	14.70	97.00	T = 45 °C, pH = 7, dose $= 1$ g/L, $C_i =$ 100 ppm	Al-Zboon et al. (2016)
Linz-Donawitz slag based	86.00	98.29	T = 44.85 °C, pH = 8, dose = 2 g/L, C <sub>i</sub> = 175 ppm	Sarkar et al. (2018)
Metakaolin based	35.88	99.08	T = not given, pH = 6–7, dose = 10 g/L, C <sub>i</sub> = 250 ppm	Andrejkovičová et al. (2016)
Metakaolin based	74.53	98.27	$T = 25 ^{\circ}\text{C},$ pH = 6.39, dose = 2  g/L, $C_i = 100$ ppm	Kara et al. (2017)
Fly ash based	47.17	87.00	$T = 25 ^{\circ}\text{C}$ pH = 6-7, dose = 1.5  g/ $L  C_i = 60$ ppm	Darmayanti et al. (2019)
Coal Gangue/ metakaolin based	11.60	80.00	$T = 50 \text{ °C}$ $pH = 6-7,$ $dose = 6 \text{ g/L}$ $C_i = 100$ $ppm$	Yan et al. (2019)
Class C Fly ash based	200	100	$T = 40 ^{\circ}\text{C},$ pH = 6, dose = 1-2  g/L, $C_i = 200$ ppm	Present study

 $C_i$  = Initial concentration of Zn.

Fig. 5c–d) with the two models, and or (ii) mass transfer limitations at different stages of adsorption, and other factors affecting the sorption process rather than pore diffusions only. However, as seen in Fig. 5a and b, the data from the third batch (i.e., 200 ppm Zn initial concentration – 1 g/L adsorbent dosage) fits fairly to the Elovich and IPD models which suggests that intra-particle diffusion plays a role in the sorption process,

in addition to chemical reaction. In some cases however, multinuclear characteristics and or low coefficient of determination indicate sorption process that is influenced by multiple processes (Fierro et al., 2008).

Previous studies have shown that Zn sorption by adsorbents fits well to Langmuir adsorption isotherm model (Al-Zboon et al., 2016; Kara et al., 2017), which assumes monolayer adsorption onto a surface with a specific number of identical sites that are homogeneously distributed over the adsorbent surface, and the energy of adsorption as equal for all sites (Chung et al., 2015; LeVan and Vermeulen, 1981; Masel, 1996). The current data is insufficient to test this isotherm and others, e.g., Freundlich adsorption isotherm model (Freundlich, 1906), however, since this aspect is well known, the focus of current study was to understand the effect of the microstructure and mineral phase assemblage (resulting from the different formulation methods) on the adsorbent performance in removing Zn.

### 3.2. Effect of microstructure and phase assemblage of adsorbents on Zn sorption

The microstructure and the phase assemblage of the adsorbents have significant impacts on their physico-mechanical and chemical properties (Mondal et al., 2020; Rakhimova and Rakhimov, 2019), and in extension affects their performance for heavy metal sorption. The SEM micrographs of the synthesized adsorbents (G1 and G2) are presented in Fig. 6a and b, showing that G1 features a coarse morphology characteristic of a phase assemblage with more crystalline compounds, compared to the G2 which shows a fine fibrous morphology indicating highly amorphous phase assemblage. The median particle size (D<sub>50</sub>) of G1 and G2 found by dynamic light scattering technique was 2324.64 nm and 1976.99 nm, respectively. Similarly, from Fig. 1b, the specific surface area of G2 (1390.43  $\text{cm}^2/\text{g}$ ), is higher than G1 (1244.63  $\text{cm}^2/\text{g}$ ), which enhances better sorption properties of G2. The FTIR spectra analyses of the prepared adsorbents (Fig. 6c) show new absorption bands at  $\sim$ 3450 cm<sup>-1</sup> and  $\sim$ 1650 cm<sup>-1</sup> which are because of O–H stretching and bending vibrations, respectively, of structural H<sub>2</sub>O and OH of the hydrated adsorbent phases; and the IR absorption band centered at  ${\sim}760~\text{cm}^{-1}$  designated for T-O of the Al–Si framework; the main Si–O-T (T = Si or Al) symmetric stretching band centered at  $\sim$ 990 cm<sup>-1</sup> and T-O stretching centered at ~450 cm<sup>-1</sup> that has become pronounced in the adsorbent samples compared to the precursor fly ash - all of these indicates the formation geopolymer-like C-(N)-A-S-H gel (Alvarez-Ayuso et al., 2008; García-Lodeiro et al., 2008; Rees et al., 2007). The absorption bands at 1435 cm<sup>-1</sup> represents C-O stretching of carbonates

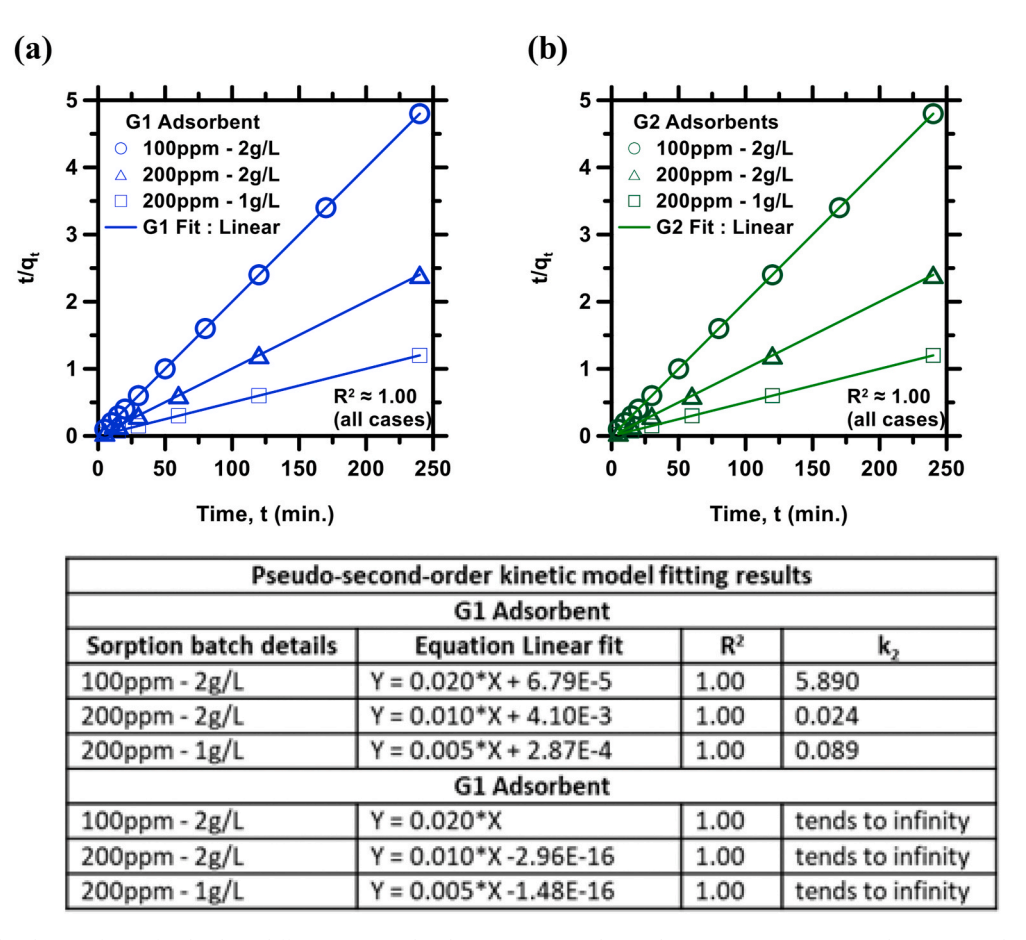


Fig. 4. Pseudo-second-order rate fitting for the three different sorption batch experiemnts with initial Zn concentrations 100 and 200 ppm and adsorbent dosages of 1 and 2 g/L, respectively: (a) G1 adsorbent; (b) G2 adsorbent: showing perfect fit to the model with  $R \sim 1.00$  in all cases.

formed due to atmospheric  $CO_2$  contamination (Álvarez-Ayuso et al., 2008; García-Lodeiro et al., 2008). It is noted that the O-H stretching and bending vibrations centered at  $\sim$ 3450 and  $\sim$ 1650 cm<sup>-1</sup> are more prominent for G1 than G2, suggesting the presence of phases imbibing more water and or hydroxyl group in the G1 assemblage. Also, there is a noticeable minor twin shoulder peaks at 1050-to-1150 cm<sup>-1</sup>, which indicates a heterogeneous gel assemblage in G1, specifically the presence of the high water-imbibing calcium silicate hydrate (C–S–H) gel (García-Lodeiro et al., 2008).

The XRD results of the precursor fly ash sample and synthesized adsorbents are shown in Fig. 7a and the percentage of amorphous gel contents estimated by quantitative XRD is presented in Fig. 7b. As the XRD patterns indicates, the G1 contains more crystalline phases originating from the hydration reaction (e.g., portlandite and sodalite; Fig. 7a) compared to the G2 which features higher amorphous contents in the hydrated phase assemblage (Fig. 7b), in agreement with the SEM image in Fig. 6. The absence of free portlandite in the XRD pattern of G2 indicates that the soluble silicate supplied by the  $Na_2SiO_3$  improved the pozzolanic reactivity of the fly ash resulting in the production of more C-(N)-A-S-H gel (Shi and Day, 1995).

Considering that fly ash hydration and the products thereof is generally limited by reactivity (Fernández-Jimenez et al., 2006; Fernández-Jiménez and Palomo, 2003; Marjanović et al., 2014; Wilińska and Pacewska, 2019), and given the evidence of unreacted fly ash in the synthesized adsorbents as indicated by the presence of quartz peaks in the XRD patterns of G1 and G2 (Fig. 7a), one may argue that the observed differences in the microstructure and phase assemblage of the adsorbents could be due to differences in the amount of fly ash reacted in each case. To elucidate the identified uncertainties, the reaction of the fly ash using the different formulation protocols used to prepare G1 and

G2 were simulated with the aid of the GEMS geochemical modeling code (described in section 2.4). Fig. 8a and b presents the evolution of hydrated phase assemblage as a function of fly ash degree of reaction. As seen in the figures, more amorphous geopolymer-like C-(N)-A-S-H gel is produced in the Na<sub>2</sub>SiO<sub>3</sub>-activated system compared to the corresponding NaOH-activated system which show higher crystalline products at each degree of fly ash reaction. Furthermore, the evolution of porosity as a function of the percentage of fly ash reacted is displayed in Fig. 8c, showing that the Na<sub>2</sub>SiO<sub>3</sub>-system features higher porosity, and based on the SEM image, the porosity is fine and evenly distributed due to the high amount of C-(N)-A-S-H gel in the microstructure - which enhances sorption (Masi et al., 2014). All of the above considerations corroborate that the higher performance of the Na<sub>2</sub>SiO<sub>3</sub>-activated fly ash (G2) is attributable to its enhanced microstructure composed of high contents of amorphous phases with improved porosity and surface area, hence providing larger number of active sites that interact with the adsorbate ion.

#### 4. Conclusions

Two different methods, NaOH-activation and  $Na_2SiO_3$ -activation, where investigated for converting high calcium fly ash (Class C fly ash) into adsorbents for the removal of aqueous Zn. While both methods produced materials with high performance in the range of 99.4-to-100% Zn removal efficiency, the adsorbent prepared with  $Na_2SiO_3$  outperformed the one prepared with NaOH, wherein the margin is much more significant in respect to sorption kinetics. The sorption kinetics and the efficiency of both materials where examined in the light of the microstructure and mineral phase assemblage observed in the materials. It was revealed that the higher performance of the  $Na_2SiO_3$ -activated

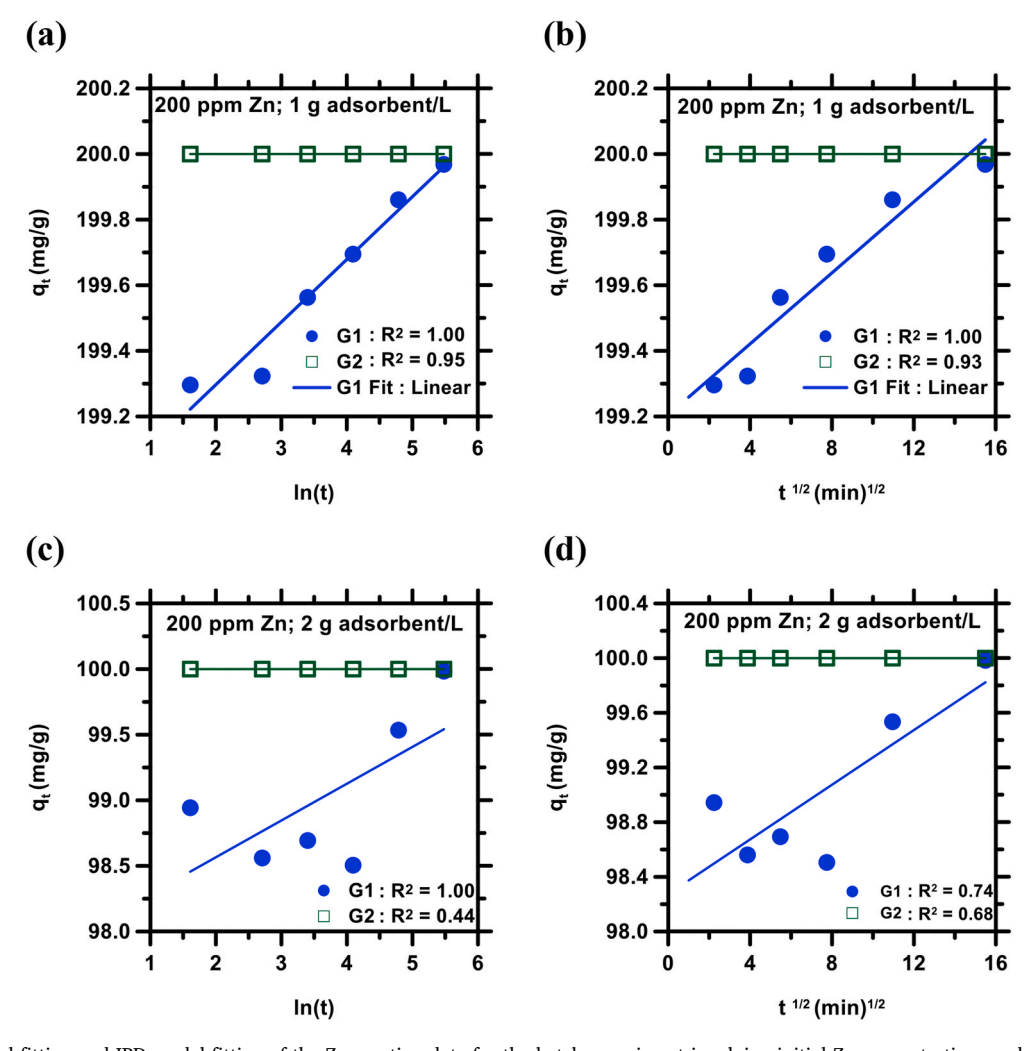


Fig. 5. Elovich model fitting and IPD model fitting of the Zn sorption data for the batch experiment involving initial Zn concentrations and adsorbent dosages of: (a–b) 200 ppm and 1 g/L; and (c–d) 200 ppm and 2 g/L, respectively.

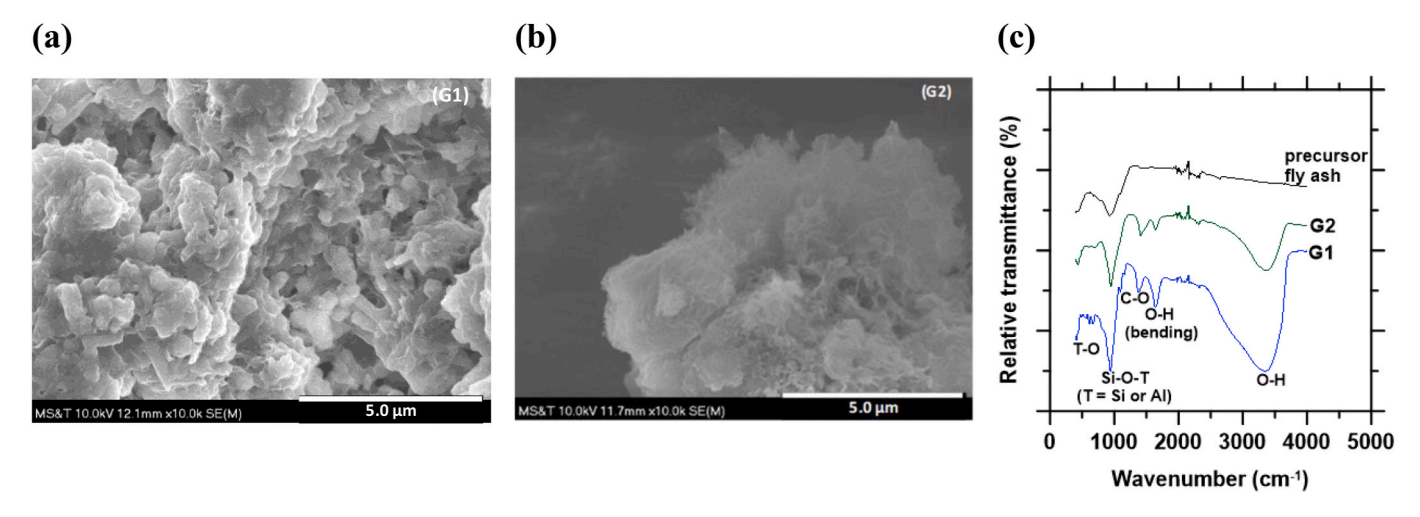


Fig. 6. SEM micrograph of synthesized adsorbents: (a) G1, (b) G2; and (c) FTIR spectra of precursor fly ash and the synthesized adsorbents.

material is due to its unique microstructure which is composed of higher contents of amorphous phase with improved porosity and surface area, thus providing more sorption sites, in contrast with the NaOH-activated material which featured higher crystalline phase assemblage and coarse morphology. The results indicate that the use of alkali-silicate activating

solution is more suitable for converting high calcium fly ash into efficient adsorbent for aqueous heavy metal sorption.

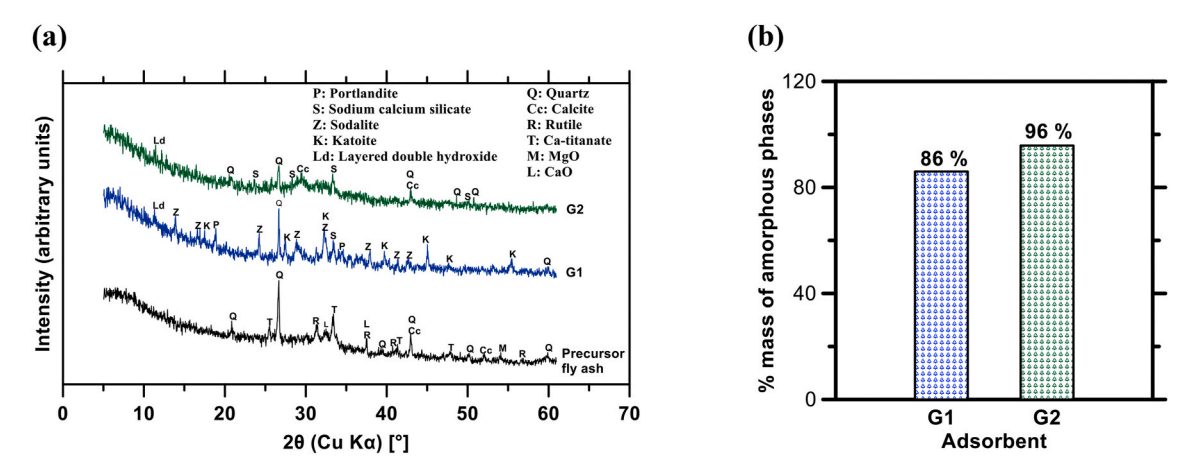


Fig. 7. (a) XRD patterns of precursor fly ash and the synthesized adsorbents, and (b) Mass percent of the amorphous phase present in each adsorbent.

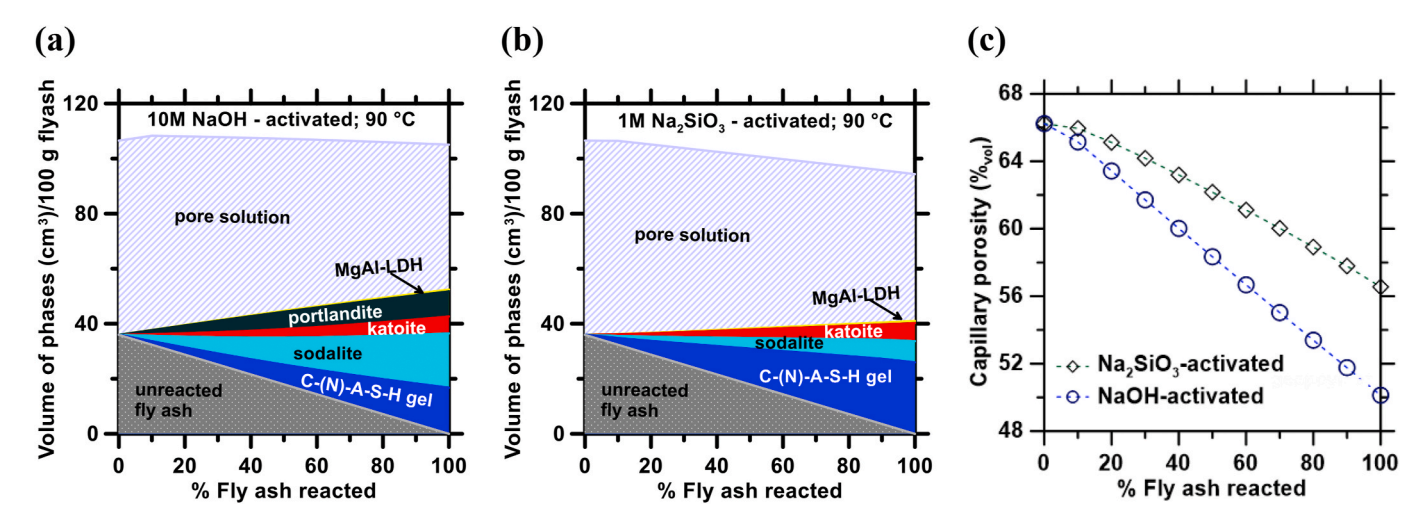


Fig. 8. The mineral phase assemblage as a function of degree of fly ash reaction: (a) NaOH-activated system, (b) Na<sub>2</sub>SiO<sub>3</sub>activated system, (c) Evolution of capillary porosity. The dotted lines are "visual guides".

#### Credit author statement

Sukanta K. Mondal: Methodology, Investigation, Formal analysis, Writing - original draft; Adam Wels: Investigation, Formal analysis; Ali Rownaghi: Writing - review & editing; Bu Wang: Writing - review & editing; Funding acquisition; Fateme Rezaei: Writing - review & editing; Validation; Aditya Kumar: Conceptualization, Writing - review & editing; Funding acquisition; Monday U. Okoronkwo: Conceptualization, Writing - review & editing, Funding acquisition, Resources, Supervision, Project administration.

#### Declaration of competing interest

The authors declare that they have no known competing financial interests or personal relationships that could have appeared to influence the work reported in this paper.

#### Acknowledgment

Funding for this study was provided by the National Science Foundation (CMMI: 1932690), and the Materials Research Center (MRC) Young Investigators' Seed Funding at Missouri S&T. The experiments were conducted at the Sustainable Materials Laboratory (SusMatLab), Materials Research Center (MRC), and at the Center for Research in Energy and Environment (CREE), all at Missouri S&T. The authors

would like to thank Lafarge Holcim, Boral Resources and Headwaters for the supply of fly as h samples.

#### References

Abu-Eishah, S.I., 2008. Removal of Zn, Cd, and Pb ions from water by sarooj clay. Appl. Clay Sci. 42, 201–205. https://doi.org/10.1016/j.clay.2008.02.003.

Adriano, D., Page, A., Elseewi, A., Chang, A., Straughan, I., 1980. Utilization and disposal of fly ash and other coal residues in terrestrial ecosystems: a review. J. Environ. Qual. 9, 333–344.

Aharoni, C., Tompkins, F., 1970. Kinetics of adsorption and desorption and the Elovich equation. Adv. Catal. 21, 1–49.

Ahmaruzzaman, M., 2010. A review on the utilization of fly ash. Prog. Energy Combust. Sci. 36, 327–363.

Ahmed, MdJ.K., Ahmaruzzaman, M., 2016. A review on potential usage of industrial waste materials for binding heavy metal ions from aqueous solutions. J. Water Process Eng. 10, 39–47. https://doi.org/10.1016/j.jwpe.2016.01.014.

Al-Harahsheh, M.S., Al Zboon, K., Al-Makhadmeh, L., Hararah, M., Mahasneh, M., 2015.
Fly ash based geopolymer for heavy metal removal: a case study on copper removal.
J. Environ. Chem. Eng. 3, 1669–1677. https://doi.org/10.1016/j.jece.2015.06.005.

Álvarez-Ayuso, E., Querol, X., Plana, F., Alastuey, A., Moreno, N., Izquierdo, M., Font, O., Moreno, T., Diez, S., Vázquez, E., Barra, M., 2008. Environmental, physical and structural characterisation of geopolymer matrixes synthesised from coal (co-) combustion fly ashes. J. Hazard Mater. 154, 175–183. https://doi.org/10.1016/j.ihazmat.2007.10.008.

Al-Zboon, K., Al-Harahsheh, M.S., Hani, F.B., 2011. Fly ash-based geopolymer for Pb removal from aqueous solution. J. Hazard Mater. 188, 414–421.

Al-Zboon, K.K., Al-smadi, B.M., Al-Khawaldh, S., 2016. Natural volcanic tuff-based geopolymer for Zn removal: adsorption isotherm, kinetic, and thermodynamic study. Water Air Soil Pollut. 227, 248.

Andrejkovičová, S., Sudagar, A., Rocha, J., Patinha, C., Hajjaji, W., da Silva, E.F., Velosa, A., Rocha, F., 2016. The effect of natural zeolite on microstructure,

- mechanical and heavy metals adsorption properties of metakaolin based geopolymers. Appl. Clay Sci. 126, 141–152.
- ASTM C618, 2019. Specification for Coal Fly Ash and Raw or Calcined Natural Pozzolan for Use in Concrete. ASTM International. https://doi.org/10.1520/C0618-19.
- Babel, S., Kurniawan, T.A., 2003. Low-cost adsorbents for heavy metals uptake from contaminated water: a review. J. Hazard Mater. 97, 219–243. https://doi.org/ 10.1016/S0304-3894(02)00263-7.
- Barakat, M.A., 2011. New trends in removing heavy metals from industrial wastewater. Arab. J. Chem. 4, 361–377. https://doi.org/10.1016/j.arabjc.2010.07.019.
- Bernal, S.A., Provis, J.L., Fernández-Jiménez, A., Krivenko, P.V., Kavalerova, E., Palacios, M., Shi, C., 2014. Binder chemistry high-calcium alkali-activated materials. In: Provis, J.L., van Deventer, J.S.J. (Eds.), Alkali Activated Materials: State-Of-The-Art Report, RILEM TC 224-AAM, RILEM State-Of-The-Art Reports. Springer Netherlands, Dordrecht, pp. 59–91. https://doi.org/10.1007/978-94-007-7672-2-2
- Blanc, P., Vieillard, P., Gailhanou, H., Gaboreau, S., Marty, N., Claret, F., Madé, B., Giffaut, E., 2015. ThermoChimie database developments in the framework of cement/clay interactions. Appl. Geochem., Geochemical Speciation Codes and Databases 55, 95–107. https://doi.org/10.1016/j.apgeochem.2014.12.006.
- Blanc, Ph, Lassin, A., Piantone, P., Azaroual, M., Jacquemet, N., Fabbri, A., Gaucher, E. C., 2012. Thermoddem: a geochemical database focused on low temperature water/rock interactions and waste materials. Appl. Geochem. 27, 2107–2116. https://doi.org/10.1016/j.apgeochem.2012.06.002.
- Bolisetty, S., Peydayesh, M., Mezzenga, R., 2019. Sustainable technologies for water purification from heavy metals: review and analysis. Chem. Soc. Rev. 48, 463–487. https://doi.org/10.1039/C8CS00493E.
- Chung, H.-K., Kim, W.-H., Park, J., Cho, J., Jeong, T.-Y., Park, P.-K., 2015. Application of Langmuir and Freundlich isotherms to predict adsorbate removal efficiency or required amount of adsorbent. J. Ind. Eng. Chem. 28, 241–246.
- Clancey, N.P., Murphy, M.C., 2012. Zinc-induced hemolytic anemia in a dog caused by ingestion of a game-playing die. Can. Vet. J. 53, 383–386.
- Darmayanti, L., Notodarmojo, S., Damanhuri, E., Kadja, G.T., Mukti, R.R., 2019.
  Preparation of alkali-activated fly ash-based geopolymer and their application in the adsorption of copper (II) and zinc (II) ions. Presented at the MATEC Web of Conferences. EDP Sciences, 06012.
- Davidovits, J., 1991. Geopolymers. J. Therm. Anal. 37, 1633–1656. https://doi.org/ 10.1007/BF01912193.
- De Gisi, S., Lofrano, G., Grassi, M., Notarnicola, M., 2016. Characteristics and adsorption capacities of low-cost sorbents for wastewater treatment: a review. Sustain. Mater. Technol. 9, 10–40. https://doi.org/10.1016/j.susmat.2016.06.002.
- Duxson, P., Fernández-Jiménez, A., Provis, J.L., Lukey, G.C., Palomo, A., van Deventer, J. S.J., 2007. Geopolymer technology: the current state of the art. J. Mater. Sci. 42, 2917–2933. https://doi.org/10.1007/s10853-006-0637-z.
- El-Eswed, B.I., 2018. Solidification versus Adsorption for Immobilization of Pollutants in Geopolymeric Materials: A Review. Solidification. https://doi.org/10.5772/
- Elouear, Z., Bouzid, J., Boujelben, N., Feki, M., Jamoussi, F., Montiel, A., 2008. Heavy metal removal from aqueous solutions by activated phosphate rock. J. Hazard Mater. 156, 412–420. https://doi.org/10.1016/j.jhazmat.2007.12.036.
- Erdem, E., Karapinar, N., Donat, R., 2004. The removal of heavy metal cations by natural zeolites. J. Colloid Interface Sci. 280, 309–314. https://doi.org/10.1016/j. icis.2004.08.028.
- Erro, A., Di Natale, F., Musmarra, D., Lancia, A., 2015. Modeling of single and competitive adsorption of cadmium and zinc onto activated carbon. Adsorption 21, 611–621
- Fernández-Jimenez, A., de la Torre, A.G., Palomo, A., López-Olmo, G., Alonso, M.M., Aranda, M.A.G., 2006. Quantitative determination of phases in the alkali activation of fly ash. Part I. Potential ash reactivity. Fuel 85, 625–634. https://doi.org/ 10.1016/j.fuel.2005.08.014.
- Fernández-Jiménez, A., Palomo, A., 2003. Characterisation of fly ashes. Potential reactivity as alkaline cements☆. Fuel 82, 2259–2265. https://doi.org/10.1016/ S0016-2361(03)00194-7.
- Fierro, V., Torné-Fernández, V., Montané, D., Celzard, A., 2008. Adsorption of phenol onto activated carbons having different textural and surface properties. Microporous Mesoporous Mater. 111, 276–284. https://doi.org/10.1016/j. micromeso.2007.08.002.
- Freundlich, H.M.F., 1906. Adsoption in solution. Phys. Chem. 57, 384-401.
- Fu, F., Wang, Q., 2011. Removal of heavy metal ions from wastewaters: a review. J. Environ. Manag. 92, 407–418.
- García-Lodeiro, I., Fernández-Jiménez, A., Blanco, M.T., Palomo, A., 2008. FTIR study of the sol–gel synthesis of cementitious gels: C–S–H and N–A–S–H. J. Sol. Gel Sci. Technol. 45, 63–72. https://doi.org/10.1007/s10971-007-1643-6.
- Ge, Y., Cui, X., Kong, Y., Li, Z., He, Y., Zhou, Q., 2015. Porous geopolymeric spheres for removal of Cu(II) from aqueous solution: synthesis and evaluation. J. Hazard Mater. 283, 244–251. https://doi.org/10.1016/j.jhazmat.2014.09.038.
- Graham, T.W., Feldman, B.F., Farver, T.B., Labavitch, F., O'Nei11, S.L., Thurmond, M.C., Keen, C.L., Holmberg, C.A., 1991. Zinc toxicosis of holstein veal calves and its relationship to haematological change and an associated thrombotic state. Comp. Haematol. Int. 1, 121–128. https://doi.org/10.1007/BF00515658.
- Graham, T.W., Goodger, W.J., Christiansen, V., Thurmond, M.C., 1987. Economic losses from an episode of zinc toxicosis on a California veal calf operation using a zinc sulfate-supplemented milk replacer. J. Am. Vet. Med. Assoc. 190, 668–671.
- Gunasekara, C., Law, D.W., Setunge, S., Sanjayan, J.G., 2015. Zeta potential, gel formation and compressive strength of low calcium fly ash geopolymers. Construct. Build. Mater. 95, 592–599. https://doi.org/10.1016/j.conbuildmat.2015.07.175.

- Gupta, S.S., Bhattacharyya, K.G., 2011. Kinetics of adsorption of metal ions on inorganic materials: a review. Adv. Colloid Interface Sci. 162, 39–58.
- Gupta, V.K., Jain, C.K., Ali, I., Sharma, M., Saini, V.K., 2003. Removal of cadmium and nickel from wastewater using bagasse fly ash—a sugar industry waste. Water Res. 37, 4038–4044. https://doi.org/10.1016/S0043-1354(03)00292-6.
- Hart, B.T., Bt, H., 1974. A Compilation of Australian Water Quality Criteria.
- He, C., Xie, F., 2018. Adsorption behavior of manganese dioxide towards heavy metal ions: surface Zeta potential effect. Water Air Soil Pollut. 229, 77.
- He, K., Chen, Y., Tang, Z., Hu, Y., 2016. Removal of heavy metal ions from aqueous solution by zeolite synthesized from fly ash. Environ. Sci. Pollut. Res. Int. 23, 2778–2788. https://doi.org/10.1007/s11356-015-5422-6.
- Hegazi, H.A., 2013. Removal of heavy metals from wastewater using agricultural and industrial wastes as adsorbents. HBRC J 9, 276–282. https://doi.org/10.1016/j. hbrci.2013.08.004.
- Helgeson, H.C., Brown, T.H., Nigrini, A., Jones, T.A., 1970. Calculation of mass transfer in geochemical processes involving aqueous solutions. Geochem. Cosmochim. Acta 34, 569–592. https://doi.org/10.1016/0016-7037(70)90017-7.
- Helgeson, H.C., Kirkham, D.H., Flowers, G.C., 1981. Theoretical prediction of the thermodynamic behavior of aqueous electrolytes by high pressures and temperatures; IV, Calculation of activity coefficients, osmotic coefficients, and apparent molal and standard and relative partial molal properties to 600 degrees C and 5kb. Am. J. Sci. 281, 1249–1516. https://doi.org/10.2475/ajs.281.10.1249.
- Ho, Y.-S., 2006. Review of second-order models for adsorption systems. J. Hazard Mater. 136, 681–689.
- Ho, Y.-S., McKay, G., 1999. Pseudo-second order model for sorption processes. Process Biochem. 34, 451–465.
- Hojati, S., Landi, A., 2015. Kinetics and thermodynamics of zinc removal from a metalplating wastewater by adsorption onto an Iranian sepiolite. Int. J. Environ. Sci. Technol. 12, 203–210.
- Hummel, W., Berner, U., Curti, E., Pearson, F.J., Thoenen, T., 2002. Nagra/PSI Chemical Thermodynamic Data Base 01/01 (No. Nagra NTB 02-16. Nagra, Wettingen, Switzerland.
- Johnson, J.W., Oelkers, E.H., Helgeson, H.C., 1992. SUPCRT92: a software package for calculating the standard molal thermodynamic properties of minerals, gases, aqueous species, and reactions from 1 to 5000 bar and 0 to 1000°C. Comput. Geosci. 18, 899–947. https://doi.org/10.1016/0098-3004(92)90029-Q.
- Juang, R.-S., Chen, M.-L., 1997. Application of the Elovich equation to the kinetics of metal sorption with solvent-impregnated resins. Ind. Eng. Chem. Res. 36, 813–820.
- Juang, R.-S., Lin, S.-H., Tsao, K.-H., 2002. Mechanism of sorption of phenols from aqueous solutions onto surfactant-modified montmorillonite. J. Colloid Interface Sci. 254, 234–241.
- Kannan, N., Sundaram, M.M., 2001. Kinetics and mechanism of removal of methylene blue by adsorption on various carbons—a comparative study. Dyes Pigments 51, 25–40.
- Kara, İ., Yilmazer, D., Akar, S.T., 2017. Metakaolin based geopolymer as an effective adsorbent for adsorption of zinc (II) and nickel (II) ions from aqueous solutions. Appl. Clay Sci. 139, 54–63.
- Kulik, D.A., Wagner, T., Dmytrieva, S.V., Kosakowski, G., Hingerl, F.F., Chudnenko, K.V., Berner, U.R., 2013. GEM-Selektor geochemical modeling package: revised algorithm and GEMS3K numerical kernel for coupled simulation codes. Comput. Geosci. 17, 1–24. https://doi.org/10.1007/s10596-012-9310-6.
- Kumar, A.S.K., Jiang, S.-J., 2016. Chitosan-functionalized graphene oxide: a novel adsorbent an efficient adsorption of arsenic from aqueous solution. J. Environ. Chem. Eng. 4, 1698–1713. https://doi.org/10.1016/j.jece.2016.02.035.
- LeVan, M.D., Vermeulen, T., 1981. Binary Langmuir and Freundlich isotherms for ideal adsorbed solutions. J. Phys. Chem. 85, 3247–3250.
- Lothenbach, B., Kulik, D.A., Matschei, T., Balonis, M., Baquerizo, L., Dilnesa, B., Miron, G.D., Myers, R.J., 2019. Cemdata18: a chemical thermodynamic database for hydrated Portland cements and alkali-activated materials. Cement Concr. Res. 115, 472–506. https://doi.org/10.1016/j.cemconres.2018.04.018.
- Malik, D.S., Jain, C.K., Yadav, A.K., 2017. Removal of heavy metals from emerging cellulosic low-cost adsorbents: a review. Appl. Water Sci. 7, 2113–2136. https://doi. org/10.1007/s13201-016-0401-8.
- Marjanović, N., Komljenović, M., Baščarević, Z., Nikolić, V., 2014. Improving reactivity of fly ash and properties of ensuing geopolymers through mechanical activation. Construct. Build. Mater. 57, 151–162. https://doi.org/10.1016/j. conbuildmat.2014.01.095.
- Masel, R.I., 1996. Principles of Adsorption and Reaction on Solid Surfaces. John Wiley & Sons.
- Masi, G., Rickard, W.D.A., Vickers, L., Bignozzi, M.C., van Riessen, A., 2014. A comparison between different foaming methods for the synthesis of light weight geopolymers. Ceram. Int. 40, 13891–13902. https://doi.org/10.1016/j. ceramint.2014.05.108.
- Mondal, S.K., Welz, A., Rezaei, F., Kumar, A., Okoronkwo, M.U., 2020. Structure–property relationship of geopolymers for aqueous Pb removal. ACS Omega 5, 21689–21699. https://doi.org/10.1021/acsomega.0c02591.
- Myers, R.J., Bernal, S.A., Provis, J.L., 2014. A thermodynamic model for C-(N-)A-S-H gel: CNASH\_ss. Derivation and validation. Cement Concr. Res. 66, 27–47. https://doi. org/10.1016/j.cemconres.2014.07.005.
- Nordberg, G., Fowler, B., Nordberg, M., 2014. Handbook on the Toxicology of Metals, fourth ed. Academic Press.
- Okoronkwo, M.U., Balonis, M., Katz, L., Juenger, M., Sant, G., 2018. A thermodynamics-based approach for examining the suitability of cementitious formulations for solidifying and stabilizing coal-combustion wastes. J. Environ. Manag. 217, 278–287. https://doi.org/10.1016/j.jenvman.2018.02.095.

- Örnek, A., Özacar, M., Şengil, İ.A., 2007. Adsorption of lead onto formaldehyde or sulphuric acid treated acorn waste: equilibrium and kinetic studies. Biochem. Eng. J. 37, 192–200.
- Pereira, C.F., Luna, Y., Querol, X., Antenucci, D., Vale, J., 2009. Waste stabilization/ solidification of an electric arc furnace dust using fly ash-based geopolymers. Fuel 88, 1185–1193.
- Plum, L.M., Rink, L., Haase, H., 2010. The essential toxin: impact of zinc on human Health. Int. J. Environ. Res. Publ. Health 7, 1342–1365. https://doi.org/10.3390/ ijerph7041342.
- Provis, J., Deventer, J. van (Eds.), 2014. Alkali Activated Materials: State-Of-The-Art Report, RILEM TC 224-AAM, RILEM State-Of-The-Art Reports. Springer Netherlands.
- Provis, J.L., 2009. Immobilisation of toxic wastes in geopolymers. In: Provis, John L., van Deventer, J.S.J. (Eds.), Geopolymers, Woodhead Publishing Series in Civil and Structural Engineering. Woodhead Publishing, pp. 421–440. https://doi.org/ 10.1533/9781845696382.3.421.
- Provis, J.L., Lukey, G.C., van Deventer, J.S.J., 2005. Do geopolymers actually contain nanocrystalline zeolites? A reexamination of existing results. Chem. Mater. 17, 3075–3085. https://doi.org/10.1021/cm050230i.
- Rakhimova, N.R., Rakhimov, R.Z., 2019. Reaction products, structure and properties of alkali-activated metakaolin cements incorporated with supplementary materials – a review. J. Mater. Res. Technol. 8, 1522–1531. https://doi.org/10.1016/j. imt. 2018.07.006
- Rattanasak, U., Chindaprasirt, P., 2009. Influence of NaOH solution on the synthesis of fly ash geopolymer. Miner. Eng. 22, 1073–1078. https://doi.org/10.1016/j. minerg/2009/03/022
- Rees, C.A., Provis, J.L., Lukey, G.C., van Deventer, J.S.J., 2007. In situ ATR-FTIR study of the early stages of fly ash geopolymer gel formation. Langmuir 23, 9076–9082. https://doi.org/10.1021/la701185g.
- Riahi, K., Chaabane, S., Thayer, B.B., 2017. A kinetic modeling study of phosphate adsorption onto Phoenix dactylifera L. date palm fibers in batch mode. J. Saudi Chem. Soc. 21, S143–S152. https://doi.org/10.1016/j.jscs.2013.11.007.
- Roy, G.M., 1994. Activated Carbon Applications in the Food and Pharmaceutical Industries, first ed. CRC Press, Lancaster.
- Sarkar, C., Basu, J.K., Samanta, A.N., 2018. Synthesis of mesoporous geopolymeric powder from LD slag as superior adsorbent for Zinc (II) removal. Adv. Powder Technol. 29, 1142–1152.
- Savaji, K.V., Niitsoo, O., Couzis, A., 2014. Influence of particle/solid surface zeta potential on particle adsorption kinetics. J. Colloid Interface Sci. 431, 165–175. https://doi.org/10.1016/j.jcis.2014.05.030.

- Shi, C., Day, R.L., 1995. Acceleration of the reactivity of fly ash by chemical activation. Cement Concr. Res. 25, 15–21. https://doi.org/10.1016/0008-8846(94)00107-A.
- Shi, G., 2019. Fly Ash-Based Geopolymer as Innovative Material for Environmental Applications (Ph.D.). Iowa State University.
- Simonin, J.-P., Bouté, J., 2016. Intraparticle diffusion-adsorption model to describe liquid/solid adsorption kinetics. Rev. Mex. Ing. Quím. 15, 161–173.
- Siyal, A.A., Shamsuddin, M.R., Khan, M.I., Rabat, N.E., Zulfiqar, M., Man, Z., Siame, J., Azizli, K.A., 2018. A review on geopolymers as emerging materials for the adsorption of heavy metals and dyes. J. Environ. Manag. 224, 327–339. https://doi.org/ 10.1016/j.jenyman.2018.07.046.
- Tan, T.H., Mo, K.H., Ling, T.-C., Lai, S.H., 2020. Current development of geopolymer as alternative adsorbent for heavy metal removal. Environ. Technol. Innov. 18 https:// doi.org/10.1016/j.eti.2020.100684.
- Thoenen, T., Humel, W., Berner, U., 2013. The PSI/nagra chemical thermodynamic database 12/07: present status and future developments. Mineral. Mag. 77, 2297–2370. https://doi.org/10.1180/minmag.2013.077.5.20.
- Uddin, M.T., Rahman, M.A., Rukanuzzaman, M., Islam, M.A., 2017. A potential low cost adsorbent for the removal of cationic dyes from aqueous solutions. Appl. Water Sci. 7, 2831–2842. https://doi.org/10.1007/s13201-017-0542-4.
- Van Jaarsveld, J., Van Deventer, J., Lukey, G., 2002. The effect of composition and temperature on the properties of fly ash-and kaolinite-based geopolymers. Chem. Eng. J. 89, 63–73.
- Wilińska, I., Pacewska, B., 2019. Comparative investigation of reactivity of different kinds of fly ash in alkaline media. J. Therm. Anal. Calorim. 138, 3857–3872. https://doi.org/10.1007/s10973-019-08296-4
- Wu, F.-C., Tseng, R.-L., Juang, R.-S., 2009a. Characteristics of Elovich equation used for the analysis of adsorption kinetics in dye-chitosan systems. Chem. Eng. J. 150, 366–373. https://doi.org/10.1016/j.cej.2009.01.014
- Wu, F.-C., Tseng, R.-L., Juang, R.-S., 2009b. Initial behavior of intraparticle diffusion model used in the description of adsorption kinetics. Chem. Eng. J. 153, 1–8. https:// doi.org/10.1016/j.cej.2009.04.042.
- Xu, D., Tan, X., Chen, C., Wang, X., 2008. Adsorption of Pb (II) from aqueous solution to MX-80 bentonite: effect of pH, ionic strength, foreign ions and temperature. Appl. Clay Sci. 41, 37–46.
- Yan, S., Zhang, F., Wang, L., Rong, Y., He, P., Jia, D., Yang, J., 2019. A green and low-cost hollow gangue microsphere/geopolymer adsorbent for the effective removal of heavy metals from wastewaters. J. Environ. Manag. 246, 174–183.
- Zhang, L., Zeng, Y., Cheng, Z., 2016. Removal of heavy metal ions using chitosan and modified chitosan: a review. J. Mol. Liq. 214, 175–191. https://doi.org/10.1016/j. molliq.2015.12.013.